A Graph-based Brain Parcellation Method Extracting Sparse Networks

Nicolas Honnorat[1], Harini Eavani[1], Theodore D. Satterthwaite[2], Christos Davatzikos[1]
[1]*Section of Biomedical Image Analysis, Department of Radiology, University of Pennsylvania*
[2]*Brain and Behavior Laboratory, Department of Psychiatry, University of Pennsylvania*
Philadelphia PA 19104, USA
Nicolas.Honnorat@uphs.upenn.edu, Harini.Eavani@uphs.upenn.edu

***Abstract*—fMRI is a powerful tool for assessing the functioning of the brain. The analysis of resting-state fMRI allows to describe the functional relationship between the cortical areas. Since most connectivity analysis methods suffer from the curse of dimensionality, the cortex needs to be first partitioned into regions of coherent activation patterns. Once the signals of these regions of interest have been extracted, estimating a sparse approximation of the inverse of their correlation matrix is a classical way to robustly describe their functional interactions. In this paper, we address both objectives with a novel parcellation method based on Markov Random Fields that favors the extraction of sparse networks of regions. Our method relies on state of the art rsfMRI models, naturally adapts the number of parcels to the data and is guaranteed to provide connected regions due to the use of shape priors. The second contribution of this paper resides in two novel sparsity enforcing potentials. Our approach is validated with a publicly available dataset.**

***Keywords*-parcellation, fMRI, Markov Random Fields, star convexity, sparsity**

I. Introduction

Resting-state fMRI (rsfMRI) has received a considerable amount of interest recently, since this imaging technique is used to describe the structure of the underlying functional networks in the cortex. Many rsfMRI analysis methods require the definition of cortical regions of interest. Typically, regions are manually delineated based on a priori knowledge. Many parcellation scheme have been proposed recently for a fully automated selection of these regions, such as [1], [2].

Graphical models are widely used for cortex parcellation [3]. Markov Random Fields (MRF) were in particular employed for rsfMRI segmentation in [4]. Most works rely on continuous parametric distributions, whose parameters are obtained using Gibbs or Monte Carlo sampling and Expectation Maximization strategies [5]. While the MRF framework provides smooth parcellations, it does not guarantee connectedness of the parcels. Once regions have been identified, the functional network can be defined using partial correlation as a measure of functional connectivity. Sparse inverse covariance estimation methods have been shown to be well suited for accurately estimating functional networks on simulated as well as clinical data [6].

In this paper, we describe a novel method for parcellating whole brain rsfMRI data that relies on discrete graphical models and aims to produce sparse networks. The segmentation is cast into an MRF framework, in which the connectedness of the parcels is enforced by star-shape priors [7], [8]. To the best of our knowledge, our approach is the first approach for functional parcellation of the entire cortex based on a discrete MRF that is guaranteed to produce connected parcels. Our method constitutes thus an alternative to normalized cuts [1], [2] and region growing [1] based methods (among others). It relies on the efficient, state of the art solvers [9], [10], [11].

Our second contribution resides in two new MRF potentials that we use for enforcing the sparsity of the correlation matrix associated with the average signal of the parcels. They are intended to indirectly sparsify the inverse of the correlation matrix (the precision matrix) that describes the interaction between the parcels [6] (when the signals are assumed to follow a Gaussian distribution). Our approach is validated on a publicly available clinical dataset.

The remainder of the paper is organised as follows. We describe our parcellation method in the section II. Section III presents the new potentials. The validation is presented in section IV and discussions conclude the paper.

II. Graph-based parcellation with shape priors

This section is devoted to the detailed description of our parcellation method. Similar to most state-of-the-art methods [1], [2], [4], this method takes as input fMRI data projected on a mesh representing the cortical surface. Let p denote a node of the mesh and l_p the parcel that contains p. We associate each parcel with a seed node that exhibits a signal similar to the average signal of the parcel and lies near the center of the parcel. Finding the parcellation of the cortex is equivalent to determining the optimal set of seeds and labels l_p. In this work, we model the labeling with a MRF containing four kinds of potentials: (1) singleton potentials $V_p(l_p)$ ensuring the coherence of the signal of the parcels (2) smoothing potentials $V_{p,q}(l_p, l_q)$ (3) label costs $V_s(\{l_p\})$ penalizing the number of parcels [12] and (4) shape priors $V_s^*(\{l_p\})$ enforcing their connectedness. As a result, the following energy is minimized:

$$E = \sum_p V_p(l_p) + \sum_{p,q} V_{p,q}(l_p, l_q) + \sum_s V_s(\{l_p\}) + \sum_s V_s^*(\{l_p\})$$

978-0-7695-5061-9/13 $26.00 © 2013 IEEE
DOI 10.1109/PRNI.2013.48

We now describe the first three potentials in the above model, that were originally proposed in [4].

A. rsfMRI Model

The likelihood that a node p belongs to a parcel l_p is modeled by a von-Mises Fisher distribution [3], [4]. As a result, we penalize the negative of the correlation coefficient between the signals of p and the seed of l_p:

$$V_p(l_p) = -\langle \mathbf{z}_p, \mathbf{z}(l_p) \rangle$$

where $\mathbf{z}_p$ is the centered and normalized signals at p and and $\mathbf{z}(l_p)$ is the signal of parcel l_p. Correlation coefficients are well suited for rsfMRI analysis and widely adopted.

Following the state-of-the-art, we control the smoothness of the segmentation with Potts potentials (where $\alpha > 0$):

$$V_{p,q}(l_p, l_q) = \begin{cases} \alpha & l_p \neq l_q \\ 0 & l_p = l_q \end{cases}$$

These potentials penalize the length of the parcels frontiers. Finally, label costs are high-order potentials involving all the l_p variables. They are particularly useful when the size of the model can vary [12]. By penalizing the use of each label, they reduce the number of parcels introduced. Since these costs are linear envelope potentials [13], they can be expressed as a sum of singleton and pairwise potentials by introducing a new variable l_s for each cost V_s that is equal to 0 when the label s is never used and to s otherwise:

$$\begin{aligned} V_s(\{l_p\}) &= V_s(l_s) + \sum_p V_{p,s}(l_p, l_s) \\ V_{p,s}(l_p, l_s) &= \begin{cases} \infty & l_p = s, l_s \neq s \\ 0 & \texttt{otherwise} \end{cases} \\ V_s(l_s) &= \begin{cases} K & l_s = s \\ 0 & l_s = 0 \\ \infty & \texttt{otherwise} \end{cases} \end{aligned}$$

B. Star-Shape Priors

The model described in the last section does not contain global geometric constraints. Hence, nothing prevents the split of parcels into disconnected components. We addressed this concern with star-shape potentials [7]. They ensure that when a node is assigned to a parcel, its shortest path to the seed is entirely included in the parcel. This condition is sufficient for guaranteeing connectedness.

In order to adapt the shape of the parcels to rsfMRI data, similar to [8], we define a geodesic distance between neighboring nodes of the mesh that depends on the correlation between their signals:

$$d_{p,q} = (1 + \beta u_{p,q})$$

where $u_{p,q} = (1 - \langle \mathbf{z}_p, \mathbf{z}_q \rangle)$ and β is a positive parameter. These distances are used for computing the shortest path between each node p and each seed s using Dijkstra's algorithm. Denoting with $\mathcal{N}(p, s)$ the neighbor of p that is the nearest to s, the star-shape potentials are given by:

$$\begin{aligned} V_s^*(\{l_p\}) &= \sum_p V_s^*\left(l_p, l_{\mathcal{N}(p,s)}\right) \\ V_s^*\left(l_p, l_{\mathcal{N}(p,s)}\right) &= \begin{cases} K^* & l_p = s, l_{\mathcal{N}(p,s)} \neq s \\ 0 & \texttt{otherwise} \end{cases} \end{aligned}$$

III. Two novel sparsity-enforcing potentials

The two novel potentials presented in this section consitute the second contribution of this work. They are designed for enforcing the sparsity of the correlation matrix S of the seeds selected during the parcellation. The first one is a parcel-level potential: it involves only the labels l_s (that are penalized by the label cost). The second one jointly involves the labels l_p and l_s.

A. Parcel-Level Sparsity Enforcing Potentials

The simplest way to sparsify S consists of penalizing one of its entrywise norms. Let us denote with $||S||_\nu$ its entrywise $\nu-$norm:

$$||S||_\nu^\nu = \sum_{i,j} |S_{i,j}|^\nu$$

We introduced for each pair of parcels $\{i, j\}$ the following pairwise potential, where λ is a positive parameter:

$$W_{i,j}(l_i, l_j) = \begin{cases} \lambda\left(|S_{i,j}|^\nu - 1\right) & l_i \neq 0,\ l_j \neq 0 \\ 0 & \texttt{otherwise} \end{cases}$$

Since $|S_{i,j}|^\nu \in [0, 1]$ and the labels l_i are only allowed two values (i or 0), these potentials are submodular. They favor segmentations with low correlation between parcels. In addition, they tend to increase the number of parcels.

B. Local Potentials

The previous potentials involve only the parcel labels. In order to involve the node variables as well and to increase the influence of the sparsity constraint, we adopted a gradient descent-like approach. We compute the gradient of the entrywise norm with respect to the matrix entries. We penalize the assignments of nodes that tend to increase the norm, because their correlations w.r.t the parcels are oriented like the gradient. This latter condition is quantified by considering the inner products between the norm gradient and the vector of the correlations between each node and the seeds. This leads to the introduction of the following potential for each node p and parcel j:

$$W_{p,j}(l_p, l_j) = \begin{cases} \eta(\langle \mathbf{z}_p, \mathbf{z}(j) \rangle \frac{\partial ||S||_\nu^\nu}{\partial S_{l_p,j}})_+ & l_p \neq j,\ l_j = j \\ 0 & \texttt{otherwise} \end{cases}$$

where $(x)_+ = max(x, 0)$, η is a positive parameter and:

$$\frac{\partial ||S||_\nu^\nu}{\partial S_{i,j}} = \nu |S_{i,j}|^{\nu-1} sgn\left(S_{i,j}\right)$$

Since the average signal of the parcels are assigned to the seeds after each iteration, favoring the inclusion of nodes weakly correlated with other parcels gradually reduces the correlations between parcels/seeds, leading to sparser S matrices. In our model, a labeling of p with l_p is penalized the most when it reinforces the correlations between l_p and the seeds j that contribute the most to the norm increase. Discarding negative values guarantees the submodularity of $W_{p,j}$. Fortunately, nodes assigned to a parcel tend to be correlated similarly as the parcel w.r.t. other parcels. Therefore, only a limited amount of values is discarded. In addition, contrary to the previous potential, this potential tends to reduce the number of parcels.

C. Selection of Seeds

Since all the potentials are submodular [1] many efficient solvers can be used for determining strong minima of our model [9], for a given set of seeds. The choice of the seeds is crucial. Our initialization strategy is presented in the validation section IV. The parcellation is performed iteratively until convergence. After each parcellation, we sample one new seed (replacing an unused seed) per parcel. The average signal over the parcel is computed. The node of the parcel that is the most correlated with this average is selected and the average signal is assigned to it. This heuristic minimizes the sum of the singleton potentials, but does not take the shape prior and the W potentials into account.

IV. Experimental Validation

A. Dataset and implementation details

We validated our approach with the pilot acquisition dataset for the *Human Connectome Project* [1], [14]. The dataset contains seven sessions (five subjects) of six ten-minutes scans (each ≈ 740 timesteps). All the scans of a session were co-registered to the corresponding structural scan and a common mesh describing the cortex was extracted using freesurfer [15]. FSL was used for processing the rsFMRI data [16]. The volumes were re-aligned to remove motion. Simultaneous confound regression [17] and band-pass filtering ($0.01 - 0.1$ Hz) was performed to remove drift. Confound regression was done with a 36-parameter model including the 6 motion parameters, the mean wm/csf/global time series as well as their temporal derivatives, the quadratic, and the quadratic of the temporal derivative. The processed fMRI data was then projected to the surface and a spatial smoothing with a Gaussian kernel of scale 4 was performed. Three corrupted scans, that our pre-processing failed to restore, were removed.

We used 400 seeds during our experiments. We sampled the first seeds by (i) computing the correlation of each node with its 250 nearest neighbors in the mesh (ii) repetitively selecting the remaining node that is the most correlated with its neighbors and discarding them. The scans of the left hemisphere of the first subject were used for setting the parameters of the segmentation to: $(K, \alpha, \beta, K^*) = (750, 0.05, 10, 15)$. The computational burden was reduced by limiting the star shape priors to a geodesic radius of 30. We used the fast approximate MRF solver FastPD [10], [11]. The same parameters $(\lambda, \eta) = (2.3, 0.125)$ (providing approximately the same number of parcels as the baseline) were used for comparing different ν-norms. We measured the sparsity of the precision matrices with the average of the absolute value of the extra-diagonal terms (normalized L1 entrywise norm). The next section presents our results.

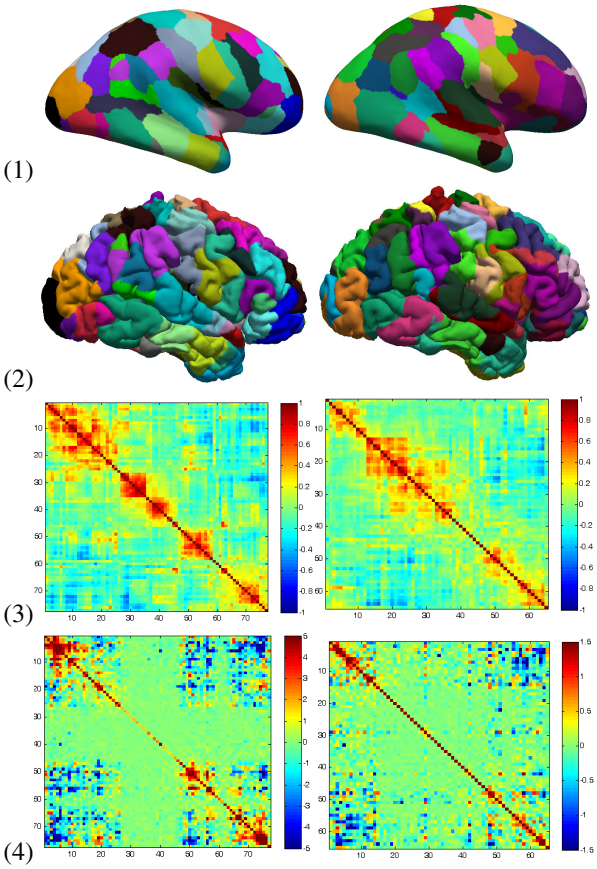

Figure 1. Left, parcellation results without sparsity enforcing potentials. Right, with $(\nu, \lambda, \eta) = (20, 2.3, 0.125)$. Row (1) inflated surface (2) cortical surface (3) correlation matrices (4) precision matrices. Each matrix has been rearranged and windowed independently for the sake of presentation.

B. Results

[Fig. (1)] illustrates the effect of the sparsity enforcing potentials on the parcellation. [Fig. (2)] presents our results. The sparsity of the precision matrix increases when ν-norms with increasing ν are considered. This result indicates that one needs to focus on reducing the largest entries of the

[1] a pairwise potential V is submodular when for any labels α, β, γ: $V(\beta, \gamma) + V(\alpha, \alpha) \leq V(\beta, \alpha) + V(\alpha, \gamma)$

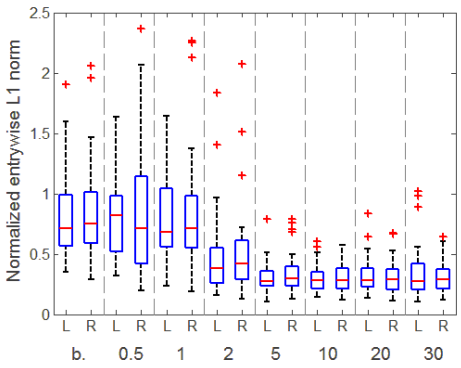

Figure 2. Normalized entrywise $L1$-norm of the extra-diagonal terms of the precision matrix obtained without sparsity constraints (baseline) or with $\nu \in \{0.5, 1, 2, 5, 10, 20, 30\}$, for the whole database. The results obtained for the left ('L') and right ('R') hemispheres are distinguished. Six scans of the left hemisphere (of the same subject) were used for parameters setting.

correlation matrix for improving the sparsity of the precision matrix. This behavior can probably be proven using the matrix blockwise inversion identity. This demonstration is however out the scope of this paper.

V. Conclusion

In this paper, we have presented a novel approach for segmenting the cortex into connected functional regions. Our method relies on a Markov Random Field that describes the fMRI signal with von-Mises Fisher distributions, determines by itself the optimal number of parcels according to a label cost and controls the smoothness of the segmentation. The connectedness of the parcels is guaranted by a star shape prior. We introduce two novel potentials. The first one acts locally and the second at the parcels level for increasing the sparsity of the correlation matrix of the model. We show that the sparsity of the inverse of the correlation matrix, that is classically considered for extracting functional networks, can be significantly increased by our approach.

Future work will focus on better sparsity enforcing potentials. Joint parcellation of multiple scans/subjects will then be addressed, which will pave the way to population studies.

References

[1] T. Blumensath, S. Jbabdi, M. F. Glasser, D. C. Van Essen, K. Ugurbil, T. E. Behrens, and S. M. Smith, "Spatially constrained hierarchical parcellation of the brain with resting-state fmri," *NeuroImage*, available online 21 March 2013.

[2] R. Craddock, G. James, P. I. Holtzheimer, X. Hu, and H. Mayberg, "A whole brain fMRI atlas generated via spatially constrained spectral clustering," *Human Brain Mapping*, vol. 33, no. 8, pp. 1914 – 1928, August 2012.

[3] D. Lashkari, E. Vul, N. Kanwisher, and P. Golland, "Discovering structure in the space of fMRI selectivity profiles," *Neuroimage*, vol. 50, no. 3, pp. 1085 – 1098, 2010.

[4] S. Ryali, T. Chen, K. Supekar, and V. Menon, "A parcellation scheme based on von mises-fisher distributions and markov random fields for segmenting brain regions using resting-state fMRI," *NeuroImage*, vol. 65, no. 0, pp. 83 – 96, 2013.

[5] W. Liu, S. P. Awate, and P. T. Fletcher, "Group analysis of resting-state fmri by hierarchical markov random fields," in *MICCAI*, 2012.

[6] G. Varoquaux, A. Gramfort, J. Poline, and B. Thirion, "Brain covariance selection: better individual functional connectivity models using population prior," in *Advances in Neural Information Processing Systems (NIPS)*, 2010.

[7] O. Veksler, "Star shape prior for graph-cut image segmentation," in *IEEE ECCV*, 2008, pp. 454 – 467.

[8] V. Gulshan, C. Rother, A. Criminisi, A. Blake, and A. Zisserman, "Geodesic star convexity for interactive image segmentation," in *IEEE CVPR*, 2010, pp. 3129 – 3136.

[9] V. Kolmogorov and R. Zabih, "What energy functions can be minimized via graph cuts?" *IEEE PAMI*, vol. 26, no. 2, pp. 147–159, 2004.

[10] N. Komodakis and G. Tziritas, "Approximate labeling via graph-cuts based on linear programming," *IEEE PAMI*, vol. 29, pp. 1436 – 1453, 2007.

[11] N. Komodakis, G. Tziritas, and N. Paragios, "Performance vs computational efficiency for optimizing single and dynamic MRFs: setting the state of the art with primal dual strategies," *Computer Vision and Image Understanding*, vol. 112, no. 1, pp. 14–29, 2008.

[12] A. Delong, A. Osokin, H. N. Isack, and Y. Boykov, "Fast approximate energy minimization with label costs." in *IEEE CVPR*, 2010.

[13] P. Kohli and M. Kumar, "Energy minimization for linear envelope MRFs," in *IEEE CVPR*, 2010, pp. 1863 – 1870.

[14] S. Smith, K. Miller, S. Moeller, J. Xu, E. Auerbach, M. Woolrich, C. Beckmann, M. Jenkinson, J. Andersson, M. Glasser, D. Van Essen, D. Feinberg, E. Yacoub, and K. Ugurbil, "Temporally-independent functional modes of spontaneous brain activity." *PNAS*, vol. 109, no. 8, pp. 3131 – 3136, 2012.

[15] A. Dale, B. Fischl, and M. Sereno, "Cortical surface-based analysis. i. segmentation and surface reconstruction." *Neuroimage*, vol. 9, pp. 179 – 194, 1999.

[16] S. Smith, M. Jenkinson, M. Woolrich, C. Beckmann, T. Behrens, H. Johansen-Berg, P. Bannister, M. De Luca, I. Drobnjak, D. Flitney, R. Niazy, J. Saunders, J. Vickers, Y. Zhang, N. De Stefano, J. Brady, and P. Matthews, "Advances in functional and structural MR image analysis and implementation as FSL," *NeuroImage*, vol. 23, no. S1, pp. 208 – 219, 2004.

[17] T. Satterthwaite, M. Elliott, R. Gerraty, K. Ruparel, J. Loughead, M. Calkins, S. Eickhoff, H. Hakonarson, R. Gur, R. Gur, and D. Wolf, "An improved framework for confound regression and filtering for control of motion artifact in the preprocessing of resting-state functional connectivity data." *Neuroimage*, vol. 64, pp. 240–256, 2013.